Optical-optical double-resonance spectroscopic study of four ion-pair states of ClF and identification of the ClF (A 3 Π 1) valence state

V. A. Alekseev and D. W. Setser

Citation: The Journal of Chemical Physics **107**, 4771 (1997); doi: 10.1063/1.474840
View online: http://dx.doi.org/10.1063/1.474840
View Table of Contents: http://scitation.aip.org/content/aip/journal/jcp/107/13?ver=pdfcov
Published by the AIP Publishing

Optical-optical double-resonance spectroscopic study of four ion-pair states of ClF and identification of the ClF($A\ ^3\Pi_1$) valence state

V. A. Alekseev[a] and D. W. Setser[b]
Chemistry Department, Kansas State University, Manhattan, Kansas 66506

(Received 29 April 1997; accepted 26 June 1997)

Four of the six ion-pair states of ClF that correlate to $Cl^+(^3P_J)$ and $F^-(^1S_0)$, the $E(0^+,{}^3P_2)$, $f(0^+,{}^3P_0)$, $\beta(1,{}^3P_2)$, and $G(1,{}^3P_1)$ states, have been identified by sequential, two-photon excitation via the ClF($B\ ^3\Pi_{0+}$) valence state. The $\Omega=1$ states, β and G, were studied by selection of rotational levels of the $B\ ^3\Pi_{0+}$ state that are perturbed by ClF($A\ ^3\Pi_1$). Spectroscopic data from laser excitation and fluorescence spectra permit the assignment of vibrational energies and rotational constants to 30 levels. These four ion-pair states exhibit extensive homogeneous and heterogeneous interactions, and neither the vibrational energy nor the rotational constants are regular with increasing vibrational quantum number. The vibrational and rotational constants of the $A\ ^3\Pi_1$ state were identified from the low resolution ClF[$\beta(1)-A\ ^3\Pi_1$] emission spectra, and the dissociation limits of the $A\ ^3\Pi_1$ and $B\ ^3\Pi_{0+}$ states are compared. The dissociation energy of ClF(X) is confirmed to be 21 110 cm^{-1}. Some qualitative information also was obtained about the $D'(2,{}^3P_2)$ and $A'\ ^3\Pi_2$ states of ClF. © *1997 American Institute of Physics.* [S0021-9606(97)01237-3]

I. INTRODUCTION

Characterization of the ion-pair and Rydberg states of halogens and interhalogens has been an active field with synergistic interactions between new experimental techniques and theoretical descriptions of the numerous potentials.[1–10] Chlorine monofluoride is the only kinetically stable fluorine-containing interhalogen diatomic molecule (BrF and IF rapidly disproportionate giving BrF_3 and IF_3). Except for a brief study of the Rydberg states,[9] the spectroscopy of high-lying electronic states of ClF has never been examined in any detail, although *ab initio* calculations of the singlet valence, Rydberg and ion-pair states have been reported.[10] According to theory,[10] avoided crossings between the Rydberg and ion-pair states of the same symmetry give double-welled potentials in the 9–10 eV range. Such potentials are of fundamental interest and they have been studied theoretically[4] and experimentally[2,3] for Cl_2. Considering the kinetic and thermal stability of ClF and the availability of theoretical treatments of the electronic structure, the lack of experimental interest in this molecule seems somewhat surprising.

In the present work, we have initiated a study of the $\Omega=0^+$ and 1 ion-pair states of ClF using the optical-optical double resonance (OODR) method. The interaction of $Cl^+(^3P_1)$ and $F^-(^1S_0)$ gives six states in Hund's case c coupling. Adopting the letter-code assignment used for other interhalogens,[5(b)] these states are given below with the number in parenthesis being the Ω values. The 0^- state has no letter assignment.

$$\begin{aligned} F^-(^1S_0)+Cl^+(^3P_2)&=D'(2,{}^3P_2),\ \beta(1,{}^3P_2),\ E(0^+,{}^3P_2)\\ &+Cl^+(^3P_1)=G(1,{}^3P_1),\ (0^-,{}^3P_1)\\ &+Cl^+(^3P_0)=f(0^+,{}^3P_0). \end{aligned} \tag{1}$$

We have identified the vibrational energies and rotational constants for the $v\leqslant 10$ levels of the $E(0^+)$, $f(0^+)$, $\beta(1)$, and $G(1)$ states, which are in the 55 000–58 000 cm^{-1} range. These levels are intrinsically interesting because of complex homogeneous and heterogeneous perturbations. Although these levels are below the range of the double-welled potentials, this information is required to build models of the ion-pair potentials that can be extrapolated to higher energy. In addition to the information about the four ion-pair states, we also report somewhat less quantitative data for the $A\ ^3\Pi_1$, $A'\ ^3\Pi_2$, and $D'(2,{}^3P_2)$ states of ClF. The relevant atomic and molecular states are shown in Fig. 1 for the convenience of the reader.

In the OODR method,[5(b)] the $B\ ^3\Pi_{0+}$, and $A\ ^3\Pi_1$ valence states are used as gateways to provide access to the ion-pair states of the halogens. The valence to ion-pair states transitions, being charge-transfer transitions along the internuclear axis, strictly follow the $\Delta\Omega=0$ selection rule and, thus, only the $\Omega=0^+$ and $\Omega=1$ ion-pair states can be probed in this way. The $0^+(^3P_0)$ and $1(^3P_1)$ states of ClF can be associated with the $^3\Sigma^-(\sigma^2\pi^2\pi^{*4}\sigma^{*2}$ and/or $\sigma^2\pi^3\pi^{*3}\sigma^{*2})$ configuration and the $0^-(^3P_1)$, $0^+(^3P_2)$, $1(^3P_2)$, and $2(^3P_2)$ states can be associated with the $^3\Pi(\sigma^1\pi^4\pi^{*3}\sigma^{*2})$ configuration. Although the potentials for these ion-pair states are similar, the different molecular orbital configurations can affect the radiative probabilities. For example, the $^3\Pi$ group of ion-pair states has an allowed one-electron transition to the excited valence $^3\Pi_{0,1,2}(\sigma^2\pi^4\pi^{*3}\sigma^{*1})$ states, whereas this transition for the $^3\Sigma^-(\sigma^2\pi^2\pi^{*4}\sigma^{*2})$ states requires a two-electron change, and other radiative transitions can be competitive or even

[a]Permanent address: Photonics Department, Institute of Physics, St. Petersburg University, 198904 St. Petersburg, Russia.
[b]Electronic mail: setserdw@ksu.edu

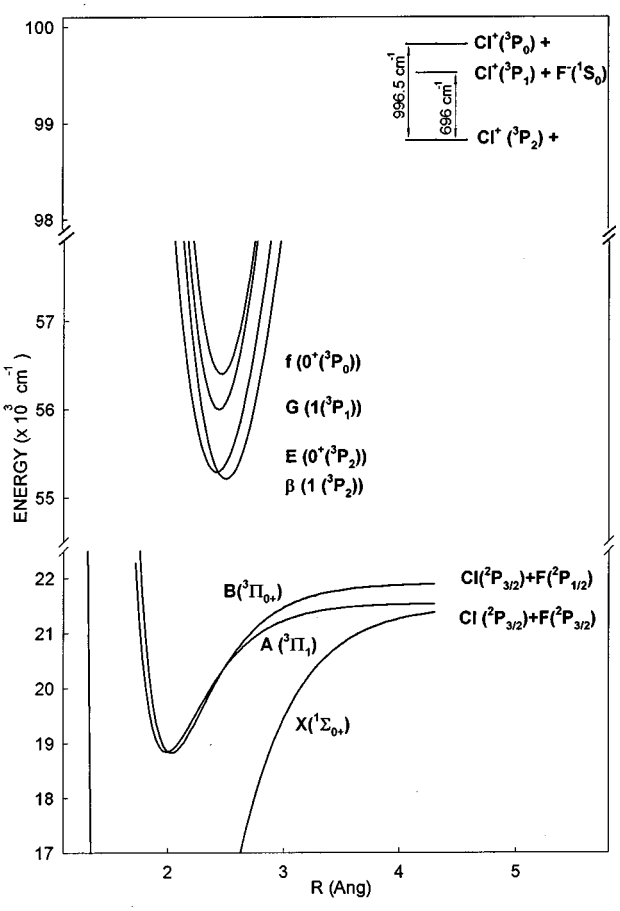

FIG. 1. Schematic representation of the atomic and molecular states of ClF. The $B\ ^3\Pi_{0+}$ potential is from Ref. 11; the $A\ ^3\Pi_1$ potential is from this work. The potentials for the ion-pair states are harmonic representations.

favored.[11] These molecular orbital configurations also affect the strength of the homogeneous perturbations, which are very important for ClF.

The excitation to the ion-pair states was performed by using the $B\ ^3\Pi_{0+}$ valence state as the intermediate.

$$^{35}\mathrm{ClF}(X)+h\nu_{\mathrm{pump}}\rightarrow{}^{35}\mathrm{ClF}(B;v,J)+h\nu_{\mathrm{probe}}\rightarrow{}^{35}\mathrm{Cl}^{+}\mathrm{F}^{-}(v',J'). \quad (2)$$

For convenience of notation, the v and J levels of $B\ ^3\Pi_{0+}$ generally will not carry a prime label when they act as intermediates; however, the conventional, double-primed notation will be used when $B\ ^3\Pi_{0+}$ state is the lower state of an emission spectrum. The pump laser was always tuned to match the transition of the ^{35}ClF isotope. Thus, the probe spectra are only for $^{35}\mathrm{Cl}^{+}\mathrm{F}^{-}$ states. Accurate spectroscopic constants of the $B\ ^3\Pi_{0+}$ state are known from McDermid's work,[11(a)] which greatly facilitated our study. Only $\Omega=0^+$ states can be probed from pure $B\ ^3\Pi_{0+}$ levels. The $\mathrm{ClF}(X\rightarrow A)$ transition seems to be extremely weak and we were unable to directly pump the $A\ ^3\Pi_1$ state. Fortunately, the $v=7$, $J=13$–15, $v=8$, $J=27$ and $v=9$, $J=10$ of $B\ ^3\Pi_{0+}$ levels are perturbed by the $A\ ^3\Pi_1$ state,[11(b)] and these perturbations allowed access to the ''e'' component of the $\Omega=1$ ion-pair states. Since the spin-orbit energies of the $\mathrm{Cl}^{+}(^3P_J)$ states are much smaller than for Br^{+} or I^{+}, the ion-pair states listed in (1) are close together in energy (see Fig. 1). The resulting strong homogeneous interaction gives irregular vibrational energies and rotational constants, and assignment of observed levels to the four states required careful evaluation; heterogeneous interaction between the $E(0^+)$ and $\beta(1)$ states makes the issue even more complex. The identification of 0^+ vs 1 states was straightforward, because (i) the latter were mainly excited via perturbed rotational levels of $B\ ^3\Pi_{0+}$ and (ii) they emit to $A\ ^3\Pi_1$ rather than to $B\ ^3\Pi_{0+}$. In order to assign a given $\Omega=0^+$ level as $f(0^+)$ vs $E(0^+)$ or a given $\Omega=1$ level as $\beta(1)$ vs $G(1)$, we depended heavily on the appearance of the fluorescence spectra. The fact that our measurements are for the ''e'' subcomponents of the $\Omega=1$ states should be remembered, because the ''f'' subcomponent should be free of heterogeneous perturbations from the $\Omega=0^+$ states.

In addition to characterizing the four ion-pair states, the low resolution $\beta(1)$, $v'-A\ ^3\Pi_1$, v'' fluorescence spectra were used to identify the vibrational levels and estimate vibrational and rotational constants of $A\ ^3\Pi_1$. The $\beta(1)-A\ ^3\Pi_1$ and $E(0^+)-B\ ^3\Pi_{0+}$ emission spectra are used to obtain the dissociation limits of the $A\ ^3\Pi_1$ and $B\ ^3\Pi_{0+}$ states. Based upon a high pressure fluorescence spectrum, the $\mathrm{ClF}[D'(2)-A'\ ^3\Pi_2]$ emission bands also were identified. In the present set of experiments, attention was focused upon the bound-bound spectroscopy; however, in the future, we hope to analyze the bound-free transitions from the $E(0^+)$, $f(0^+)$, $\beta(1)$, and $G(1)$ states to the repulsive valence states.[12]

II. EXPERIMENTAL METHODS

The output of a XeCl excimer laser (Questek 2840) was divided with a beam splitter and used to pump two Lambda-Physik dye lasers. The fundamental output of the first dye laser, LPD2002, was used to excite a selected rotational level of $v=6$ or 7 of $\mathrm{ClF}(B\ ^3\Pi_{0+})$. Coumarin 480 and 503 dyes were used for the 470–550 nm range needed for the $B\leftarrow X$ transition; the temporal half-width of laser pulse was ~15 ns and the energy was ~1–3 mJ. The doubled output of a second dye laser, LPD3002, with Coumarin 540 was used for the 290–265 nm range of the probe step. The half-width of this laser pulse was also ~15 ns and the energy per pulse was 0.1–0.3 mJ. The two laser beams were directed into the laser-induced fluorescence gas cell from opposite directions. No explicit time delay between the two laser pulses was used for most experiments. The cell was attached to the entrance flange of the monochromator and the laser beams were aligned so as to be overlapped in front of the entrance slit of the monochromator. A 0.5 or 1 m focal length lens was used for each laser beam to increase the efficiency of excitation.

The gas cell was constructed from stainless steel and had 25-cm-long baffle arms. The ClF(Ozark Mahoning) was used in natural isotopic abundance without further purification. The typical pressure of ClF was in the 1–5 Torr range. In a fully passivated cell, the ClF pressure remained constant for many hours without any noticeable decomposition. The fluo-

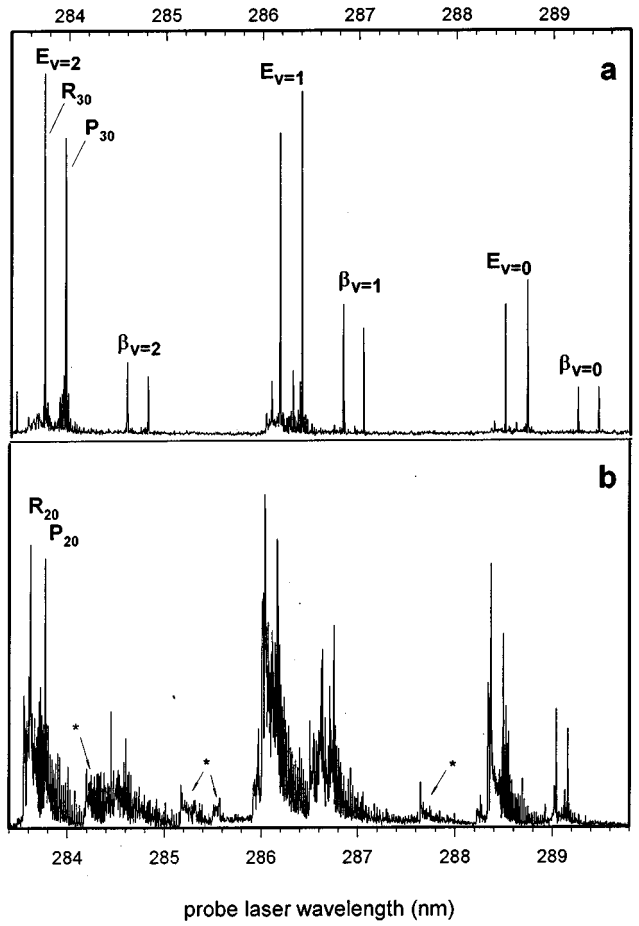

FIG. 2. (a) Low resolution (0.5 nm) excitation spectrum from a ClF (2 Torr)+Xe(1 Torr) mixture. The pump laser was tuned to the ($X\ ^1\Sigma^+, v''=0, J''=29 \rightarrow B\ ^3\Pi_{0+}, v'=7, J'=30$) transition. (b) Low resolution excitation spectrum from a ClF (2 Torr)+Xe(10 Torr)+He(50 Torr) mixture. The pump laser was tuned to the ($X\ ^1\Sigma^+, v''=0$, $J''=19 \rightarrow B\ ^3\Pi_{0+}, v'=7$, $J''=20$) transition. The extended rotational structure demonstrates the rotational relaxation of ClF ($B\ ^3\Pi_{0+}, v'=7$). The weak bands marked with the asterisk are from lower levels formed by vibrational relaxation of ClF ($B\ ^3\Pi_{0+}, v'=7$).

rescence was observed through a quartz window attached to the cell; the distance between the window and the entrance slit of the monochromator was ~0.5 cm and light collecting optics were unnecessary. The monochromator, 0.5 m Minuteman, was equipped with a 1200 g/mm grating blazed at 300 nm and Hamamatsu R955 photomultiplier tube. The output signal of the photomultiplier tube was digitized with Hewlett-Packard 54510A digital storage oscilloscope and transferred to a computer for storage and analysis. The radiative decay rates of the ClF ion-pair states were very fast with ~80% of the intensity emitted during the time of the laser pulse. Our results are consistent with radiative lifetimes of ~10 ns or less, which is normal for halogen and interhalogen ion-pair states.[5(b)]

In the OODR technique, the rovibronic levels of the ion-pair states are excited from a selected v,J level of $B\ ^3\Pi_{0+}$ (or $A\ ^3\Pi_1$) prepared by the pump laser. Such an experiment is usually performed at low pressure to avoid collisional relaxation in the $B\ ^3\Pi_{0+}$ (or $A\ ^3\Pi_1$) state, and an excitation spectrum typically displays a sequence of P-R doublets [see Fig. 2(a)] for excitation to v', $J'=J\pm1$ levels of the ion-pair states. This experiment must be repeated several times with different J to collect data to derive spectroscopic constants. In the present work, we used rotational relaxation in the $B\ ^3\Pi_{0+}$ state via collisions with He to accelerate the data acquisition [see Fig. 2(b)]. A typical experimental mixture for recording excitation spectra consisted of ClF (1–3 Torr), He(~50 Torr), and Xe(~10 Torr). The role of Xe was to provide a monitor for the ClF ion-pair states using the reactive quenching reaction

$$Cl^+F^- + Xe \rightarrow XeCl(B,C) + F. \tag{3}$$

The XeCl(B) state gives strong fluorescence in the 308 nm range where the scattered laser light intensity was low. A typical low-resolution excitation spectrum obtained in this way is shown in Fig. 2(b). In comparison with the spectrum taken without He [Fig. 2(a)], this spectrum displays a developed rotational structure that demonstrates the extent of rotational relaxation. Several examples of high resolution excitation spectra will be presented below. The wavelengths of the pump and probe lasers were calibrated from the known wavelengths of the ClF(B-X) absorption spectra.[13] The accuracy of the wavelength assignments of the high resolution excitation spectrum is determined by the effective resolution of the laser scan ($0.3\ cm^{-1}$).

The fluorescence spectra were recorded with the 0.5 m monochromator from 2 Torr of pure ClF. Since the rotational relaxation in the upper ion-pair state was negligible, these fluorescence spectra are from specific J' levels. The signals actually were strong and the resolution was normally 2 Å corresponding to a slit width of 0.1 mm. Some $\beta(1)$-$A\ ^3\Pi_1$ fluorescence spectra were taken in the second order to resolve the P and R lines. The wavelength scale of the monochromator was calibrated from the wavelength of the scattered laser light.

III. EXPERIMENTAL RESULTS

A. Assignment of vibrational levels to the $\beta(1,{}^3P_2)$ and $G(1,{}^3P_1)$ states

The initial search for $B\ ^3\Pi_{0+} \rightarrow E(0^+)$, $\beta(1)$, $f(0^+)$, and $G(1)$ resonances was carried out in the $h\nu_{pump} + h\nu_{probe} = 55\,000$–$62\,000\ cm^{-1}$ range, and ~70 vibrational levels were found. Because of the interactions between these states, the vibrational progressions were strongly irregular and assignment of the observed resonances was difficult. Due to this reason, efforts were concentrated on the more narrow $h\nu_{pump} + h\nu_{probe} = 55\,000$–$58\,000\ cm^{-1}$ range. The vibrational levels observed in this range are presented in Table I and Fig. 3(a). After a resonance was identified, high resolution excitation spectra, see Fig. 4, were taken to identify the origin of the band and to assign the rotational constants given in Table I and shown in Figs. 3(b) and 3(c). The $\Omega=1$ states could be easily distinguished from the $\Omega=0^+$ states, based on the $\beta(1)$, $G(1) \rightarrow A^3\Pi_1$ fluorescence spectra,

TABLE I. Spectroscopic constants for the ClF (E, f, β, and G) states.

v'	$E(0^+,{}^3P_2)$	$f(0^+,{}^3P_0)$	$\beta(1,{}^3P_2)$	$G(1,{}^3P_1)$
	55 289.3[a]	56 237.0	55 212.9	56 024.1
0	0.2339[b]	0.2264	0.2181	0.230
	−4[c]	±1	4	n/d[d]
	55 573.0	56 653.1	55 503.6	56 452.9
1	0.2335	0.2242	0.2230	0.226
	±1	±1	5	n/d
	55 876.0	57 050.8	55 774.1	56 851.3
2	0.2296	0.2214	0.226	0.227
	±1	±1	2.5	n/d
	56 173.9	57 485.5	56 077.7	57 224.1
3	0.2265	0.2248	0.223	0.223
	±1	4	n/d	n/d
	56 492.9	57 856.2	56 391.5	57 573.0
4	0.2272	0.2212	0.2197	0.222
	−3	−2	±1	n/d
	56 812.8	58 225.7	56 712.4	57 907.5
5	0.2258	0.2174	0.217	0.221
	±1	±1	n/d	n/d
	57 138.0		57 040.6	
6	0.2253		0.218	
	±1		n/d	
	57 413.9		57 380.1	
7	0.2193		0.216	
	±1		n/d	
	57 744.6		57 732.5	
8	0.2202		0.209	
	±1		n/d	
	58 064.3			
9	0.2141			
	±1			

[a]Energy (cm^{-1}) of level relative to $X(v''=0)$; the absolute uncertainty was estimated as $\pm 2\ cm^{-1}$, the uncertainty for the energy separations between successive levels is $\sim 0.5\ cm^{-1}$. The absolute uncertainty includes the uncertainty in our assignment of the high resolution excitation spectra (see footnote b) plus the uncertainty in the energy of the $B\ {}^3\Pi_{0+}$ level (Ref. 11).

[b]Rotational constant (cm^{-1}). The estimated uncertainty of the rotational constant is ~0.2% for the $E(v')$, $f(v')$, and $\beta(v'=0,$ 1, and 4) levels and ~1% for the other β and G levels. The uncertainty in the fitting of the rotational line positions was determined by the effective resolution of the UV probe laser, which was $0.3\ cm^{-1}$. Thus, the assignment of the origin should be good to $\leqslant 0.5\ cm^{-1}$. The B_v and D_v values were obtained by visually matching the line positions of the entire set of rotational lines in a simulated (calculated) spectrum with the experimental spectrum.

[c]Distortion constant D ($10^{-7}\ cm^{-1}$). Limit of measurable value of distortion constant in the present experiments was $\pm 1\times 10^{-7}\ cm^{-1}$, and an entry of ±1 means that the distortion constant was within this range.

[d]The entry n/d means no data available. Spectroscopic constants for these levels were estimated from the position of a single P-R doublet originating from a perturbed level of B, $v''=7$.

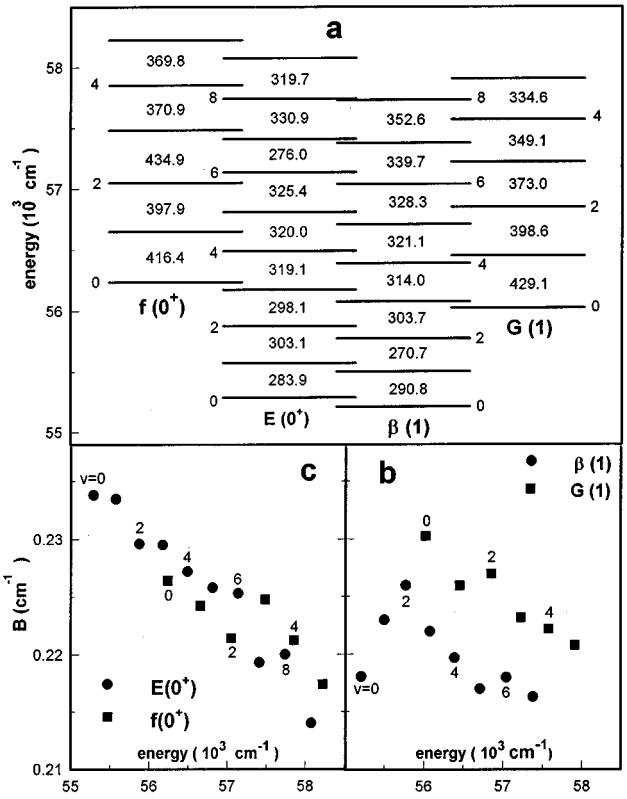

FIG. 3. (a) Schematic diagram of the vibrational levels of the ClF ion-pair states observed in the present work. The numbers between successive levels are the energy separation (cm^{-1}). (b) and (c) The rotational constants for the $\beta(1)$, $G(1)$, $E(0^+)$, and $f(0^+)$ vibrational levels. The B_v values are plotted vs the total energy.

vide infra. The rotational structure of the excitation spectra for the $\Omega=1$ levels was also less developed than for $\Omega=0^+$ states.

A characteristic difference between the excitation spectra for the low v' levels of $\beta(1)$ and all levels of $G(1)$ at the same He pressure is the more extended rotational structure for $\beta(1)$, as illustrated in Fig. 4. The P and R transitions from the laser prepared $B^3\Pi_{0+}(v=7,J=20)$ level are the most intense lines in both spectra. In addition, transitions from the perturbed $^3\Pi_{0+}$ levels, $J=13$–15, also are strong in both the $\beta(1;v'=0)$ and $G(1;v'=3)$ spectra. However, the transitions for $J'>20$ are very weak for $G(v'=3)$. This difference between $\beta(1;v'=0-3)$ and $G(1;v'=0-3)$ excitation spectra is a consequence of a J-dependent interaction between the $\beta(1;v'=0-3)$ and $E(0^+;v'=0-3)$ levels. This interaction mixes the $\Omega=0^+$ and $\Omega=1$ states, which allows $\Delta\Omega=1$ transitions, but with the same selection rules as for the $\Delta\Omega=0$ transitions (i.e., without a Q branch transition). The band head is absent in both spectra, which implies that low J' transitions have weak oscillator strength [see Sec. III describing the $E(0^+)$ and $f(0^+)$ rotational spectra at the same He pressure for comparison].

The rotational constants for individual v' levels were assigned from the excitation spectrum using the combination difference relation, Eq. (4), for the P and R lines

$$R(J)-P(J)=4B'_{v'}(J+\tfrac{1}{2}). \tag{4}$$

For spectra with more fully developed structure, all rotational lines were used in the analysis and Eq. (5) was employed

$$\nu=\nu_0+(B'_{v'}+B_v)m+(B'_{v'}-B_v-D'_{v'}+D_v)m^2 -2(D'_{v'}+D_v)m^3-(D'_{v'}-D_v)m^4. \tag{5}$$

In Eq. (5), $m=-J$ for the P branch and $m=J+1$ for the R branch; the constants for the $B^3\Pi_{0+}$ state were taken from Ref. 13. Because of the strong P and R doublets originating from the laser-prepared $B\ {}^3\Pi_{0+}(v,J)$ level, the absolute

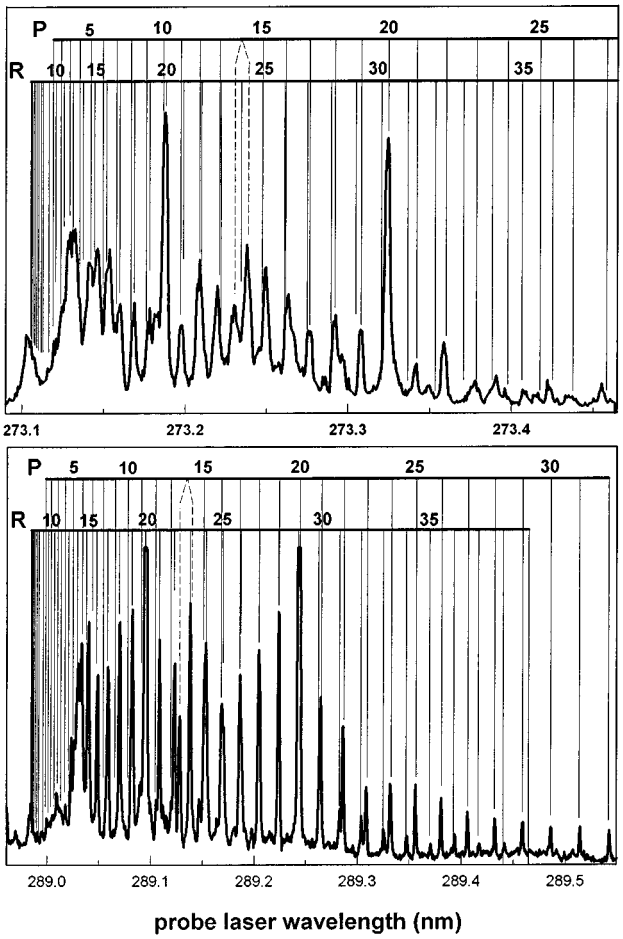

FIG. 4. High resolution excitation spectra of the $\beta(1)$, $v'=0 \leftarrow B\ ^3\Pi_{0+}$, $v=7$, bottom, and $G(1)v'=3 \leftarrow B\ ^3\Pi_{0+}$, $v=7$, top, bands obtained from a ClF (3 Torr)+Xe(10 Torr) and He(50 Torr) mixture. The pump laser was tuned to the $(X\ ^1\Sigma^+, v''=0, J''=19 \rightarrow B\ ^3\Pi_{0+}, v'=7, J'=20)$ line; the transitions are labeled by the rotational level of the $B\ ^3\Pi_{0+}$ state. Note the enhanced intensity for the $J=13-15$ transitions, which is a consequence of perturbations between the ClF($B\ ^3\Pi_{0+}$ and $A\ ^3\Pi_1$) states. Transition from both components of the $J=14$ level are shown in the P branch by the dashed lines.

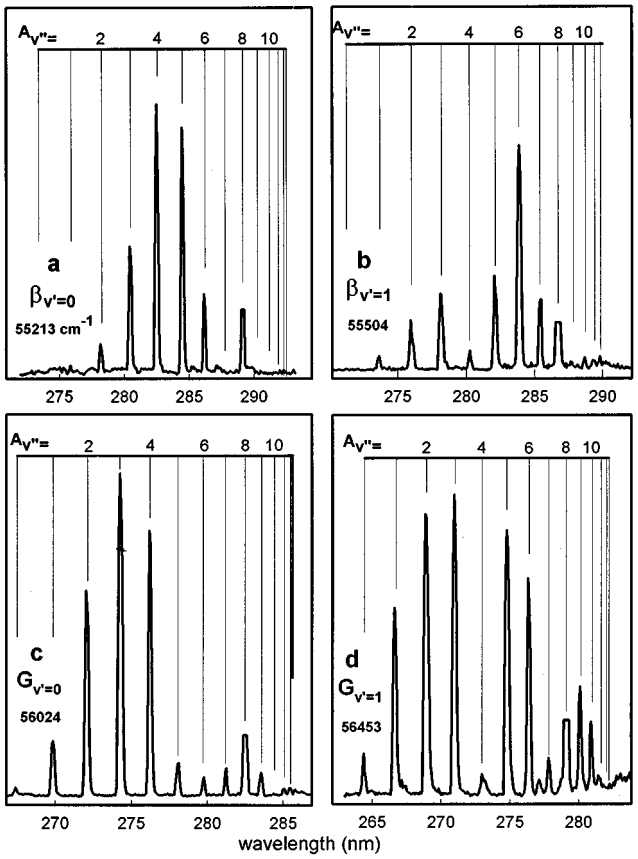

FIG. 5. Fluorescence spectra of $\beta(1)$, $v'=0$ and 1 and $G(1)$, $v'=0$ and 1 from pure ClF at 1 Torr. The excitation sequence was $X \rightarrow^{(0\rightarrow 7)R_{13}} B \rightarrow^{(7\rightarrow 0\ or\ 1)R_{14}} \beta$ (or G). Note that the $\beta(1)$ and $G(1)$ state emit to $A\ ^3\Pi_1$ and not $B\ ^3\Pi_{0^-}$. The truncated bands are the bands that are concident with the scattered light.

numbering of the lines in the excitation spectra is easily established. The majority of the rotational constants for the $\beta(1)$ and $G(1)$ in Table I were assigned using Eq. (4) and the $B_{v'}$ values are reported to only three significant figures. The data for ($\beta 1; v'=0$, 1, and 2) levels were sufficient to define their distortion constants, $D_{v'}$.

The vibrational numbering of the $\beta(1)$ and $G(1)$ levels was assigned from low resolution fluorescence spectra from experiments at 2 Torr of ClF. The ion-pair states have larger R_e than the $A\ ^3\Pi_1$ or $B\ ^3\Pi_{0+}$ states and the fluorescence intensities are modulated according to the probability distribution determined by the upper state vibrational wave functions. As an example, fluorescence spectra from the vibrational levels at 55 213, 55 504, 56 024, and 56 453 cm^{-1} are shown in Fig. 5. These $\beta(1)$ and $G(1) \rightarrow A\ ^3\Pi_1$ emission spectra can be used to characterize the $A\ ^3\Pi_1$ state (see below). The 55 213 and 55 504 cm^{-1} levels, which are the two lowest ones of the $\Omega=1$ manifold and the emission intensities display, respectively, a single and double maximum. Thus, these levels can be assigned unambiguously to $v'=0$ and $v'=1$ of $\beta(1)$. Comparison of the spectra in Figs. 5(a) and 5(b) show that the 56 024 and 56 453 cm^{-1} levels can be assigned as $v'=0$ and 1 of $G(1)$.

The systematic difference in $B_{v'}$ values for pairs of levels with close absolute energies [see Figs. 3(b) and 3(c)] was the main criteria used to identify levels as members of the $G(1)$ and $\beta(1)$ manifolds for energies above 56 600 cm^{-1}. The outer turning point is more extended for higher v' levels, which gives a broader Frank–Condon range for the bound-bound transitions and more intense bound-free emissions [the $\beta(1; v'=8)$ spectrum is shown in Fig. 9]. The bound-free emission includes transitions to $A\ ^3\Pi_1$ that terminate above the dissociation limit plus transition in the 300–380 nm range to repulsive potential(s).[12] The $G(1; v')$ states have higher relative contributions to the latter than do the $\beta(1; v')$ states.

B. Assignment of the ClF($A\ ^3\Pi_1$) vibrational and rotational constants

The $\beta(1)$, $v'=0,1,2 - A\ ^3\Pi_1, v''$ emission spectra together with selected $G(1)$, $v' - A\ ^3\Pi_1, v''$ spectra clearly

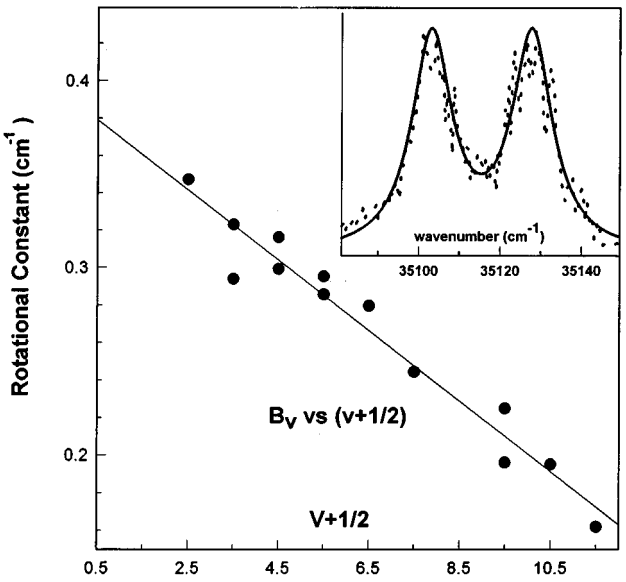

FIG. 6. Plot of B_v values for $A\ ^3\Pi_1$ vs $v+1/2$. The B_e and α_e values are 0.39 ± 0.01 and 0.019 ± 0.001, respectively. The $\beta(1)$, $v'=0$, $J'=19\rightarrow A\ ^3\Pi_1$, $v''=5$, $J''=J'\pm1$ doublet is shown in the insert as an example of the data. The line fits the smoothed data. The v'' levels with two data points include experiments from two different v'. The disparity in the points illustrates the uncertainty in the B_v values.

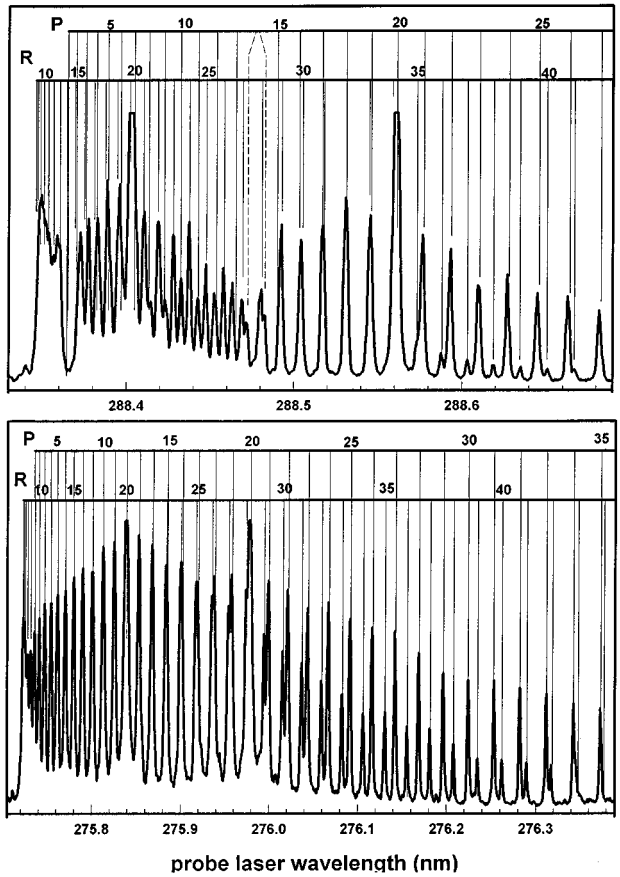

FIG. 7. High resolution excitation spectra for $E(0^+)$, $v'=0\leftarrow B\ ^3\Pi_{0+}$, $v=7$, top, and $f(0^+)$, $v'=1\leftarrow B\ ^3\Pi_{0+}$, $v=6$, bottom, from a ClF(3 Torr)+Xe(10 Torr)+He(50 Torr) mixture. Spectra were acquired with the pump laser tuned to $X\ ^1\Sigma^+$, $v''=0$, $J''=19\rightarrow B\ ^3\Pi_{0+}$, $v'=7$, $J'=20$ and $\rightarrow B\ ^3\Pi_{0+}$, $v'=6$, $J'=20$. Transition from both components of the $J=14$ level are shown for the P branch by dashed lines in the top spectrum. The transitions are labeled by the rotational level of the $B\ ^3\Pi_{0+}$ state.

identified transitions to the $v''=0-12$ levels. The P and R transitions from $\beta(1)$, $v'=2$ and 4, $J'=19\rightarrow A\ ^3\Pi_1$, $v''=2-11$ were resolved by using the monochromator in the second order. From the wavelengths of the separated P and R lines and Eq. (4), the rotational constants of the $A\ ^3\Pi_1$ state were evaluated. Least-square fitting of the data shown in Fig. 6 gave $B_e=0.39\pm0.01$ and $\alpha_e=0.019\pm0.001$. The rotational constants were used together with the positions of the resolved P and R doublets from $J'=19$ to estimate the band origin of the vibrational bands. Based upon the $v''=0-10$ data, the vibrational constants of the $A\ ^3\Pi_1$ state are $T_e=18841\pm5$, $\omega_e=353\pm1$, $\omega_e x_e=9.7\pm0.1$, $\omega_e y_e=0.17\pm0.02\ \mathrm{cm}^{-1}$ with $R_e=1.87$ Å. The energies (2354 ± 5 and $2411\pm5\ \mathrm{cm}^{-1}$ above $A\ ^3\Pi_1, v''=0$) of the $v''=11$ and 12 bands, which were estimated from the positions of the origins, did not fit the power series expression, and they were not included in the fitting of the vibrational constants. For comparison, the corresponding constants for ClF ($B\ ^3\Pi_{0+}$) are $T_e=18\,825.3$, $\omega_e=363.1$, $\omega_e x_e=8.64$, $\omega_e y_e=0.124\ \mathrm{cm}^{-1}$, and $R_e=2.03$ Å. The $A\ ^3\Pi_1$ state correlates to $\mathrm{Cl}(^2P_{3/2})+\mathrm{F}(^2P_{3/2})$ and the vibrational levels extend smoothly to the dissociation limit; see spectrum in Fig. 5. In contrast, the $B\ ^3\Pi_{0+}$ state correlates to $\mathrm{Cl}(^2P_{3/2})+\mathrm{F}(^2P_{1/2})$ and it is predissociated at $v=9$, $J\geqslant21$ and $v=10-13$ by the $Y(0^+)$ potential, which correlates to $\mathrm{Cl}(^2P_{3/2})+\mathrm{F}(^2P_{3/2})$. However, the $E(0^+)$ and $f(0^+)\rightarrow B\ ^3\Pi_{0+}$ emission spectra have bands that extended to $v''=10-13$, *vide infra*.

C. Assignment of vibrational levels to the $E(0^+,{}^3P_2)$ and $f(0^+,{}^3P_0)$ states

Our approach to the analysis of the 0^+ states was the same as just described for the $\beta(1)$ and $G(1)$ states. After the resonances were found, high resolution excitation spectra were taken and examples are shown in Fig. 7. The rotational structure is completely developed, and these spectra demonstrate the extensive rotational relaxation of the pumped $B\ ^3\Pi_{0+}$ level in 50 Torr of He. The more constrained range of J observed for the $\beta(1;v')$ and $G(1;v')\leftarrow B\ ^3\Pi_{0+}$ transitions of Fig. 4 is associated with an intrinsic dependence of the Einstein coefficients on the rotational quantum number.

The B'_v, and D'_v, values for $E(0^+)$ and $f(0^+)$ are listed in Table I and Fig. 3. These constants were obtained from fitting the line positions in the excitation spectra to standard expression for P and R branches given in Eq. (5). The B_0 and B_1 values of $E(0^+)$ are anomalously large, presumably because of heterogenous perturbations with the $v'=0$ and 1 levels of $\beta(1)$; see Sec. IV. The $B_{v'}$ values for $v'=0-2$ of $f(0^+)$ and some intermediate $E(0^+)$ levels decline in a more-or-less regular way, but an abrupt shift occurs at $f(0^+;v=3)$ and $E(0^+;v=7)$. Unlike the $\beta(1)$ vs $G(1)$ case, the $E(0^+)$ and $f(0^+)$ levels with close absolute energy do not display systematic differences in their rotational constants, and additional criteria are needed to sort the

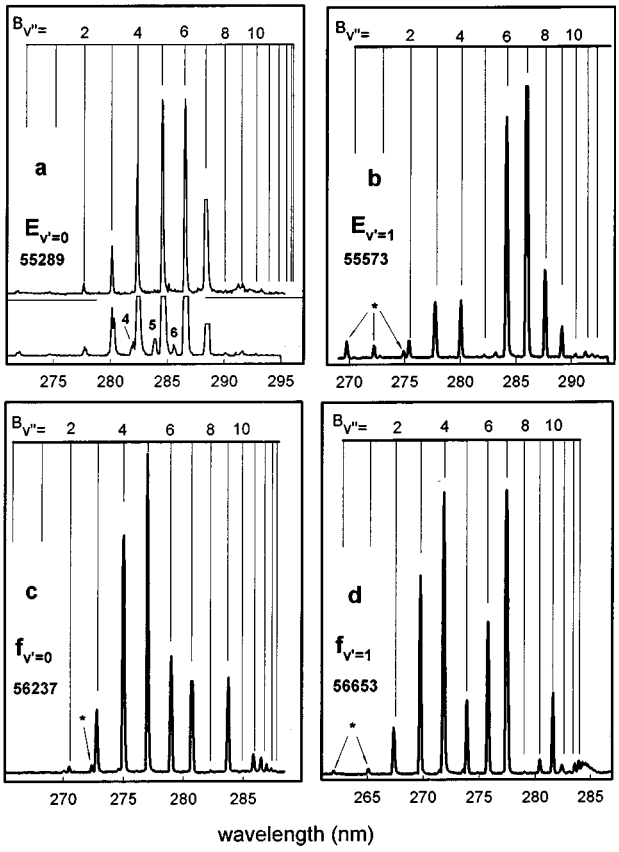

FIG. 8. Fluorescence spectra of $E(0^+)$,$v'=0$ and 1 and $f(1)$, $v'=0$ and 1 from pure ClF at 1 Torr. The excitation sequence was $X\rightarrow^{(0\rightarrow 7)R_4}B\rightarrow^{(7\rightarrow 0\ or\ 1)P_5}E$ (and f). The lines marked with the asterisk were assigned as transitions to high levels of the ClF ($X\ ^1\Sigma^+$) ground state. The second spectrum at the bottom of (a) was obtained from excitation to $E(0^+;v'=0)$, $J'=19$. The weak bands marked as 4, 5, and 6 are transition to $^3\Pi_1$ $A(v''=4$, 5, and 6) that illustrate the J-dependent heterogeneous mixing between $E(0^+)$ and $\beta(1)$.

$E(0^+;v')$ and $f(0^+;v')$ levels. These criteria are discussed in the next paragraph.

The fluorescence spectra in Fig. 8 display the intensity modulations expected for emission from $v'=0$ and 1 levels, although the relatively strong $v''=9$ and 10 bands from the $f(0^+;v'=0$ and 1) levels are somewhat surprising (see Sec. IV). Thus, the 55 289 and 55 573 cm^1 levels can be assigned to $E(0^+)$ and the 56 237 and 56 653 cm^{-1} levels to $f(0^+)$. The larger R_e for the $f(0^+)$ state, relative to the $E(0^+)$ state, is evident from the emission bands that extend to the dissociation limit of ClF($B\ ^3\Pi_{0+}$) for the former. Transitions to these high v'' bands also were observed in emission for $E(0^+;v'\geqslant 2$ levels). With the above assignment for the $v'=0$ and 1 energies of $f(0^+)$, the 55 876 and 56 174 cm^{-1} levels must be the $v'=2$ and 3 levels of $E(0^+)$.

Assignment of the vibrational number based on the intensity modulation of the bound-bound spectra for $v'\geqslant 2$ levels is not so obvious, since the number of nodes is comparable with the number of observed bands. The separations between the vibrational levels in the $f(0^+)$ state, although irregular, are appreciably larger than in $E(0^+)$ state (see Fig. 8), which provides identification for the $f(0^+;v'=2)$ and $E(0^+;v'=4$ and 5) levels. A decision must be made for the 57 414 and 57 485 cm^{-1} levels. If the former is assigned as $E(0^+;v'=7)$ and the latter as $f(0^+;v'=3)$, then the spacing between $E(v'=6$ and 7) is anomalously small and the spacing between $f(v'=2$ and 3) is anomalously large. A similar dichotomy exists between the B_v values [see Fig. 3(c)].

The $B\ ^3\Pi_{0+}$ state is relatively shallow, $D_e=3079.1\ cm^{-1}$ with a smaller R_e than for the ion-pair states. Due to this reason, a substantial part of the $E(0^+;v')$ and $f(0^+;v')\rightarrow B\ ^3\Pi_{0+}$ emissions for $v'>4$ are actually bound-free. Since the molecular orbital configurations of the $E(0^+)$ and $f(0^+)$ states are different, the bound-free emission spectra from higher v' levels to $B\ ^3\Pi_{0+}$ or to other 0^+ repulsive valence states could differ for $E(0^+)$ vs $f(0^+)$. The fluorescence spectra from the next two levels at 57 856 and 57 745 cm^{-1} are compared in Fig. 9. The higher bound-free emission intensity from the 57 745 cm^{-1} level together with the more numerous oscillations in the 280–290 nm range (which is the bound-free emission to $B\ ^3\Pi_{0+}$) suggests that this level has the larger vibrational quantum number, i.e., it is $E(0^+;v'=8)$. The bound-free emission actually extends to 380 nm, and the long wavelength intensity from the 57 856 and 57 485 cm^{-1} levels is somewhat more intense than that of the 57 445 cm^{-1} level, in accord with a molecular orbital description that differs from $E(0^+)$. Such arguments were used to assign the highest three vibrational levels in the $E(0^+)$ and $f(0^+)$ states. The similarity of the long wavelength part of the bound-free emission spectra from $\beta(1;v'=8)$ and $E(0^+;v'=8)$ in Fig. 9 should be noted. The intensity of the bound-free continua, relative to the bound-bound spectrum, is much stronger for the $E(0^+)$ state. These observations suggest that this particular bound-free emission from $\beta(1)$ might be a consequence of heterogeneous mixing with $E(0^+)$. This similarity exists for other pairs of high levels of $\beta(1)$ and $E(0^+)$ with the same v.

An alternative way to confirm the absolute vibrational numbering is to measure the isotope shifts from the ^{37}ClF spectra. Such work is in progress[12] and the vibrational numbering adopted for the levels in Table I seems to be satisfactory.

IV. DISCUSSION

A. The ClF($A\ ^3\Pi_1$) state and the bond dissociation energy of ClF($X\ \Sigma^+$)

From the convergence limit (21 514±2) of the $X\ ^1\Sigma^+\rightarrow B\ ^3\Pi_{0+}$ absorption spectrum,[11(c)] the bond dissociation energy of ClF(X) can be assigned as either 20 633 on 21 110 cm^{-1}, depending upon whether $F(^2P_{3/2})+Cl^*(^2P_{1/2})$ or $F^*(^2P_{1/2})+Cl(^2P_{3/2})$, respectively, is the dissociation limit for the $B\ ^3\Pi_{0+}$ state. The experimental ClF($B\ ^3\Pi_{0+}$) predissociation limit[11](a) also gives an absolute upper limit of $D_0(X)=21\ 126\pm 6\ cm^{-1}$. Our $E(0^+)$ and $f(0^+)\rightarrow B\ ^3\Pi_{0+}$,$v''$ spectra clearly establish that $B\ ^3\Pi_{0+}$ dissociates to $F^*(^2P_{1/2})+Cl(^2P_{3/2})$. Thus, the best measurement of $D_0(X)$ is 21 110±2 cm^{-1} from the convergence

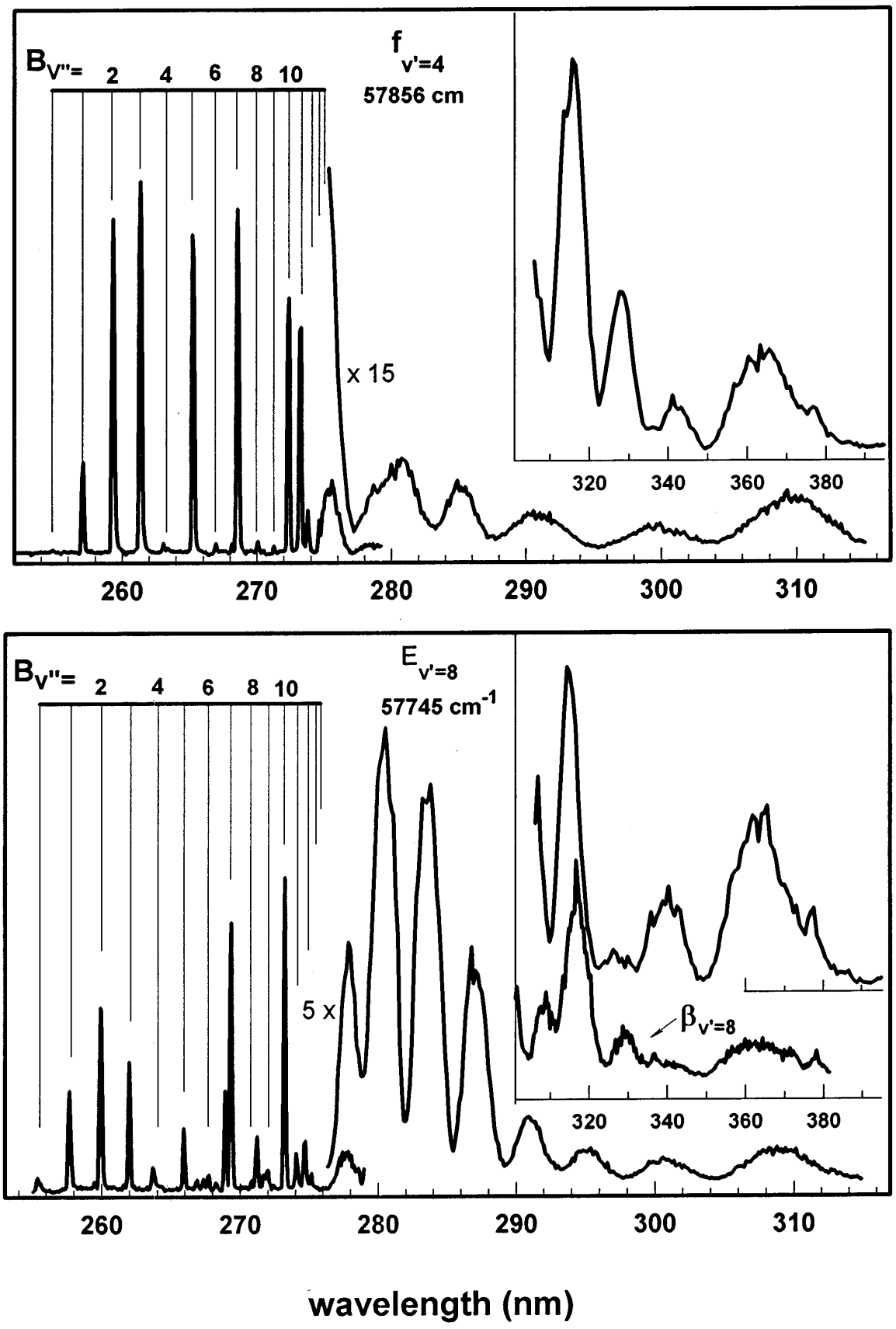

FIG. 9. Fluorescence spectra from $E(0^+)$, $v'=8$, $J'=6$ and $f(1)$, $v'=4$, $J'=6$. Note the difference in the bound-free emission pattern from these levels in the range of 276–290 nm, but the overall similarity of the bound-free emission in the long wavelength range shown in the insert. The emission in the long wavelength range from $\beta(1)$, $v'=8$, $J'=13$ is shown to illustrate some common features with the emission from $E(0^+)$, $v'=8$.

limit. This value is also consistent with the highest level ($v=12$) observed for $A\ ^3\Pi_1$, i.e., $T_0+E_{12}=18\,624+2365=20\,989\ \mathrm{cm}^{-1}$. The $\beta(1)\rightarrow A\ ^3\Pi_1$ spectrum shows additional unresolved emission. If the $\Delta G(v+1/2)$ values for $A\ ^3\Pi_1$ are linearly extrapolated to zero on a $v+1/2$ plot, the energies for $v=13$ and 14 can be estimated. These estimates add $69\ \mathrm{cm}^{-1}$ to $D_0(A\ ^3\Pi_1)$ and give $D_0(X)\geqslant 21\,058\ \mathrm{cm}^{-1}$. The highest resolved band in our $E(0^+)$, $f(0^+)\rightarrow B\ ^3\Pi_{0+}$ spectra was $v''=14$. The sum of T_0+E_{14} is $21\,446\ \mathrm{cm}^{-1}$, subtracting the energy ($404\ \mathrm{cm}^{-1}$) difference between $F(^2P_{3/2})$ and $F(^2P_{1/2})$ gives $D_0(X)=21\,042\ \mathrm{cm}^{-1}$. Strickler and Krauss[11(c)] report absorption spectra to $v'=15$, 16, and 17 and, if their energies are included, the $D_0(X)$ increases to the value derived from the convergence limit. We conclude that the dissociation energies of the $X\ ^1\Sigma^+$, $A\ ^3\Pi_1$, and $B\ ^3\Pi_0$ states are internally self-consistent.

According to our results, the difference in T_0 for the $A\ ^3\Pi_1$ and $B\ ^3\Pi_{0+}$ states is only $20\ \mathrm{cm}^{-1}$, even though the R_e of $A\ ^3\Pi_1$(1.87 Å) is smaller than for $B\ ^3\Pi_{0+}$(2.03 Å). Rydberg–Klein–Rees (RKR) calculation were performed to compare the potentials of the $A\ ^3\Pi_1$ and $B\ ^3\Pi_{0+}$ states; see Fig. 1. The abnormally large α_e for $A\ ^3\Pi_1$ state leads to a very hard repulsive wall. Since $A\ ^3\Pi_1$ correlates to the lower asymptote, the outer limb of the $A\ ^3\Pi_1$ potential cuts across the $B\ ^3\Pi_{0+}$ potential. We suspect that our α_e value may be too large and higher resolution data from a broader range of rotational levels are needed to provide more reliable rotational constants. The shapes of the $A\ ^3\Pi_1$ and $B\ ^3\Pi_{0+}$ potentials probably are more similar than the current data for $A\ ^3\Pi_1$ suggest.

B. The $E(0^+,{}^3P_2)$, $\beta(1,{}^3P_2)$, $G(1,{}^3P_1)$, and $f(0^+,\ {}^3P_0)$ ion-pair states

Due to the irregular nature of the vibrational energy levels and B_v values, assignment of representative ω_e and R_e value for the Cl^+F^- states is not possible. Nevertheless, the mid-range levels of $E(0^+)$ and $\beta(1)$ suggest a ω_e value near $320\ \mathrm{cm}^{-1}$ and extrapolation of the rotational constants suggests $R_e\equiv 2.42$ Å. The $\beta(1)$ state is the lowest energy state of these four ion-pair states and the dissociation energy to $Cl^+(^3P_2)+F^-$ is $43\,612\ \mathrm{cm}^{-1}$. The ion-pair states of ClF have the largest bond dissociation energy of the halogen and interhalogen ion-pair states (with the exception of F^+F^-).

The most striking feature of the halogen and interhalogen ion-pair states is the overall similarity of the potentials, which are of the general Rittner form,[3(b)] for the different Ω states of a given halogen.[1–10] The spread in R_e is usually less than 3% and the spread in D_e (or T_e) for states correlating to the same positive-ion state is ~2%. It follows that the ion-pair potentials cluster in groups separated by the spin-orbit energies of the $X^+(^3P_2,\ ^3P_1,\ ^3P_0,$ and $^1D_2)$ states. The Cl^+F^- states also fit this pattern. The energy separation between the $v=0$ levels of the $E(0^+)$ and $f(0^+)$ states, $948\ \mathrm{cm}^{-1}$, is close to the difference, $996\ \mathrm{cm}^{-1}$, between the $Cl^+(^3P_2)$ and $Cl^+(^3P_0)$ states; however, the separation between the $v=0$ levels of $\beta(1)$ and $G(1)$, $812\ \mathrm{cm}^{-1}$, matches less closely the separation, $696\ \mathrm{cm}^{-1}$, between $Cl^+(^3P_2)$ and $Cl^+(^3P_1)$. Comparison of the Cl^+F^- and Cl^+Cl^- states is useful. The energy separation between the $^3\Pi_g(2_g,1_g,0_g^+)$ group and the (1_g and 0_g^+) group for $Cl_2(\sim 1600\ \mathrm{cm}^{-1})$[1(d)] is much larger than for the Cl^+F^- state. In fact, the $948\ \mathrm{cm}^{-1}$ separation for the Cl^+F^- states more closely resembles the separation for the $^3\Pi_g$ and $^3\Sigma_u^-$ states of Cl_2.[1(a)] This observation implies that the best orbital description for the $f(0^+)$ and $G(1)$ states of Cl^+F^- is $\sigma^2\pi^3\pi^{*3}\sigma^{*2}$, which also is consistent with the observation that the strengths of the $f(0^+)\rightarrow B\ ^3\Pi_{0+}$ and $G(1)\rightarrow A\ ^3\Pi_1$ transitions are comparable to the $E(0^+)\rightarrow B\ ^3\Pi_{0+}$ and $\beta(1)$-$A\ ^3\Pi_1$ transitions. Thus, both sets of transitions presumably are one-electron change processes. Although all of the $^3\Pi_g$ and $^3\Sigma_g^+$ states of Cl^+Cl^- are regular, the $[^3\Pi(1_u,{}^3P_2)$ and $^3\Sigma^-(1_u,{}^3P_1)]$ and the $[^3\Pi(0_u^+,{}^3P_2)$ and $^3\Sigma^-(0_u^+,\ {}^3P_0)]$ pairs exhibit irregular vibrational spacings with states correlating to the $Cl^+(^3P_1)$ and $^3P_0$ limits having larger spacings than those correlating to $Cl^+(^3P_2)$. This is the same pattern as for Cl^+F^- states. The electron configurations of the $^3\Pi(0_u^+,1_u)$ and $^3\Sigma^-(0_u^+,1_u)$ states of Cl_2 differ by permutation of one electron $\sigma^1\pi^3\pi^{*4}\sigma^{*2}$ and $\sigma^2\pi^3\pi^{*3}\sigma^{*2}$, respectively, and these states exhibit strong interactions. In contrast, the $^3\Pi_g$ $(\sigma^1\pi^4\pi^{*3}\sigma^*)^2$ and $^3\Sigma_g^-$ $(\sigma^2\pi^2\pi^{*4}\sigma^*)^2$ states of Cl_2 being different by permutation of two electrons, do not interact.[1] According to this analysis, the $^3\Pi(0^+,1)$ states of Cl^+F^- with a $\sigma^1\pi^4\pi^{*3}\sigma^{*2}$ configuration interact with the $^3\Sigma^-(0^+,1)$ states with the $\sigma^2\pi^3\pi^{*3}\sigma^{*2}$ configuration.

The large vibrational frequency, but with a large apparent anharmonicity, for the $G(1)$ and $f(0^+)$ levels contrasts with the small vibration frequency and apparent negative anharmonicity for the $\beta(1)$ and $E(0^+)$ levels of Cl^+F^- [see Fig. 3(a)]. Pairwise interaction between close lying energy levels cannot explain this irregular pattern. This is especially obvious from the smaller separation between $v=0$ and 1 vs $v=1$ and 2 of $E(0^+)$, although $f(0^+)$ has no levels in the vicinity of $E(0^+,\ v=1$ or 2). Apparently, a much broader range of levels must be involved in the homogenous interaction. A model based upon two equivalent zero-order harmonic potentials (with ψ_v^0 and ϕ_v^0 vibrational wave functions) with a constant interaction strength H^e, modified by the overlap integral, provides some insight into the experimental energy level patterns. As a first approximation, the shift of a level v_1 due to interaction with all levels of the other electronic state can be written as Eq. (6)

$$\delta E_{v1}=\sum_{v2}\left(\frac{-\Delta E_{v_1,v_2}}{2}\pm\sqrt{\left(\frac{\Delta E_{v_1,v_2}}{2}\right)^2+H_{v_1,v_2}^2}\right), \quad (6)$$

$$H_{v_1v_2}=H^e\langle\psi_{v_1}^0\phi_{v_2}^0\rangle. \quad (7)$$

The v_1 and v_2 designate the vibrational levels in the two different electronic states, $\Delta E_{v_1,v_2}$ is the energy separation between the zero-order energy levels and the upper and lower signs are for the cases $\Delta E_{v_1,v_2}>0$ and $\Delta E_{v_1,v_2}<0$, respectively; H^e is the electronic part of the matrix element, which to a first approximation was taken as a constant. The sets of states for $H^e=0$ and H^e $250\ \mathrm{cm}^{-1}$ are shown in Fig.

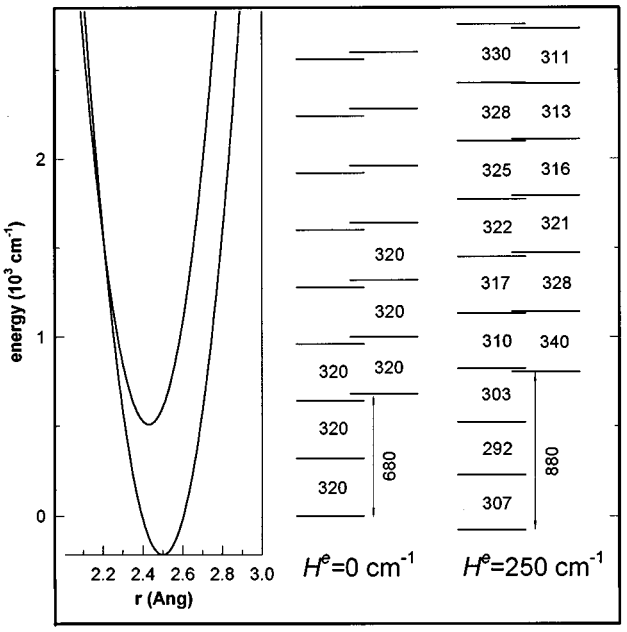

FIG. 10. Schematic diagram to illustrate the consequences of homogenous interactions between a range of levels represented as harmonic oscillators for the two potentials shown in the insert. The two sets of levels are for $H^e=0$ and $H^e=250\ \mathrm{cm}^{-1}$. The two zero-order potentials are separated by $680\ \mathrm{cm}^{-1}$. (See the text for other details.)

10. The choice for $\Delta R_e(\sim 3\%)$ was made from consideration of the experimental values for the $\beta(1)$ and $G(1)$ states and ΔT_e was taken as the energy separation between Cl^+ ($^3P_2$ and $^3P_1$). The basis set included 20 vibrational levels in each state. This set was adequate for the calculation of δE_{v_1}, since the overlap integrals between levels with $\Delta v > 10$ are negligible for our choice of ΔT_e and ΔR_e.

Although such calculations are sensitive to the parameter for the zero-order levels and to the difference in R_e values, comparison of Figs. 10 and 3(a) show that the calculation does qualitatively match the experimental pattern of irregular vibrational levels. A more quantitative deperturbation analysis requires a better model for the zero-order states, which should be based on Rittner potentials that would give more accurate overlap integrals. In the present calculations, the value of $250\ \mathrm{cm}^{-1}$ for H^e was chosen empirically. Some change in H^e is expected for better basis potentials. Shifts of a wide range of vibrational levels resulting from interactions between two electronic states of the same symmetry is discussed by Lefebvre-Brion and Field.[14] Multilevel interaction models have been developed to explain such perturbations,[14] and the discussion given in Ref. 15(a) for the SiO case resembles the energy level pattern for ClF.

The multilevel homogeneous interactions discussed above are largely responsible for the irregular vibrational level pattern of the $E(0^+)$ and $f(0^+)$ states, as well as for $\beta(1)$ and $G(1)$. However, the $E(0^+)$ and $f(0^+)$ levels seem to exhibit additional complications. The B_v for the $f(0^+;v'=0-2)$ are systematically smaller than for the $E(0^+)$ states. Thus, the R_e for $f(0^+)$ is larger than for $E(0^+)$ and a possibility exists for an avoided crossing of these two potentials at the outer turning point. The abrupt shift in the order of the B_v values for $f(0^+;v'=3)$ and $E(0^+;v'=7)$ suggest that a crossing (or avoided crossing) may occur at this energy. Another possibility could be the overtaking of levels in one manifold by the other, see Fig. 10 with an abrupt change in the relative contributions of the mixing coefficients. A full deperturbation analysis is required to provide a better explanation.

The multilevel perturbations mix the vibrational wave functions and the first[14(c)] approximation to the wave function for a perturbed level is given by Eq. (8)

$$\psi_{v_1}=C_{v_1,v_1}\psi_{v_1}+\sum_{v_2} C_{v_1,v_2}\phi^0_{v_2}. \tag{8}$$

The $\psi^0_{v_1}$ and $\phi^0_{v_2}$ are the zero-order wave functions and C_{v_1,v_2} is the normalized mixing coefficient. This mixing will affect the vibrational band intensities in the emission spectra. In particular emission spectra from the two upper ion-pair states, $f(0^+)$ and $G(1)$ [Figs. 5(c), 5(d), 8(c), and 8(d)] show intensity modulations that are unusual for pure vibrational $v=0$ and 1 wavefunction. Mixing is also responsible for transitions to a broader range of v'' levels observed in the spectra from $v'=0$ and 1 of $f(0^+)$ and $G(1)$, relative to the spectra from these levels of $E(0^+)$ and $\beta(1)$ (compare the upper and lower panels of Figs. 5 and 8). Since ω_e is larger for $f(0^+)$ and $G(1)$ than for $E(0^+)$ and $\beta(1)$, the upper pair of potentials are more narrow than the lower pair and, in the absence of mixing, the range of v'' transitions from $f(0^+)$ and $G(1)$ would be more restricted, rather than broader, relative to $E(0^+)$ and $\beta(1)$.

The multilevel homogeneous mixing also will affect the B_v values. The definition[14(c)] of B_{v_1} for the i level shows that the mixing will contribute to the irregular behavior

$$B_i=\sum_{n=1,2}\sum_{vn}|C_{i,vn}|^2 B_{vn} \tag{9}$$

of the B_v values shown in Figs. 3(b) and 3(c). The pattern for $\beta(1)$ and $G(1)$ does seem to reflect this perturbation, because the first two B_v values are lower (and higher) than expected from the overall trend in the B_v values for $\beta(1)$ and $G(1)$. However, the B_v for $\beta(1)$ and $E(0^+)$ states also can be affected by heterogeneous interactions.

Heterogeneous perturbations between the ion-pair states correlating to $X^+(^3P_2)$ is thoroughly documented.[5,6,15] The states of this cluster perturb each other through coriolis interaction, which splits the doubly degenerate sublevels of the $\Omega=2$ and 1 states (often called Ω doubling). The strength of this coriolis interaction increases with J. The heterogenous interaction for ClF is evident from the weak $E(0^+)\rightarrow A\ ^3\Pi_1$ and $\beta(1)\rightarrow B\ ^3\Pi_{0+}$ radiative transitions [see Figs. 8(a) and 11] and from the rotationally enhanced excitation spectra for $\beta(1;v'=0,1)$ (Fig. 4). The shift in energy of the e sublevels of $\beta(1)$ from the f sublevels is given by Eq. (10).[5(d)] The $E(0^+)$ levels are shifted by an equal amount in the opposite direction

$$\Delta E=(B_e-B_f)J(J+1)\approx(12B^2f_{vv'}^2/\Delta G)J(J+1). \quad (10)$$

The terms have the following definitions: $\Delta G=G_{\beta,v}-G_{E,v}$, $f_{vv'}=\langle\psi_v(\beta)|\psi_v(E)\rangle$, and $B=(B_\beta+B_E)/2$. The induced separations[5,6] between the e and f sublevels are usually less than 1 to 2 cm^{-1}, but these shifts do affect the apparent B_v and D_v values.[5,6,15] Since $E(0^+,v'=0)$ is above $\beta(1;v'=0)$, this heterogeneous interaction increases $B_0(E)$ and decreases $B_0(\beta)$. For $f_{vv}^2=1$, the upper limit to the change in B_v values is 0.008 cm^{-1}, which is large enough to explain the anomalous B_v values for the three lowest levels of the $\beta(1)$ and $E(0^+)$ states. The heterogeneous mixing between $\beta(1)$ and $E(0^+)$ declined with vibrational energy, as demonstrated by the absence of $\beta(1)\rightarrow B\ ^3\Pi_{0+}$ and $E(0^+)\rightarrow A\ ^3\Pi_1$ transitions from higher v' levels, and by the much narrower range of J' levels observed for the $(\beta,v'\leftarrow B,v'')$ excitation spectra. In order to separate the contributions from homogeneous and heterogeneous perturbations to the measured values of B_v for $\beta(1)$ and $E(0^+)$ states, experimental measurements for the heterogeneously unperturbed f sublevels of $\beta(1)$ are needed.

C. The ClF [$D'(2,^3P_2)$-$A'\ ^3\Pi_2$] spectrum

Considering the similarity of the ion-pair states, the potential for ClF($D',^3P_2$) should provide a good approximation for the deperturbed potentials of the $E(0^+)$, $f(0^+)$, $\beta(1)$, and $G(1)$ states. Unfortunately, the $\Delta\Omega=0$ selection rule forbids direct access to the $D'(2)$ state from $B\ ^3\Pi_{0+}$. An attempt to use the perturbed rotational levels of $B\ ^3\Pi_{0+}(v'=7)$ was not successful. This experiment and the fact that emission from $\beta(1;v'=0)$, see the center spectrum of Fig. 11, shows no bands that terminate in $A'\ ^3\Pi_2$ (although very weak $\beta(1)\rightarrow B\ ^3\Pi_{0+}$ bands can be seen) suggests that the heterogenous mixing between $\beta(1)$ and $D'(2)$ is weak. We also tried to collisionally generate a sufficient concentration in the $A'\ ^3\Pi_2$ for subsequent excitation to $D'(2)$. In this experiment, the pump laser was tuned to the band head of X, $v''=0\rightarrow B$, $v'=4$ transition and 300 Torr of He (or CF_4) was added to provide the collisional relaxation. A 10 m optical path for the UV laser beam was used to obtain a 30 ns time delay between the pump and probe laser pulses. The resulting excitation spectra consisted of several weak and badly overlapped bands that could not be easily identified or analyzed. Since the Franck–Condon factors for transitions from the lowest levels of the valence states to the lowest levels of the ion-pair states are small, the method may be more successful for investigation of higher levels of $D'(2)$.

Excitation of high pressures of ClF buffer-gas mixtures has given laser action;[16,17] however, spectroscopic analysis of the emission spectra from the ion-pair states has not been done. We excited the $E(0^+;v'=0)$ level in 300 Torr of CF_4 to obtain the emission spectrum from a 300 K Boltzmann distribution among the $D'(2)$, $\beta(1)$, and $E(0^+)$ states. The spectra from individual $\beta(1;v'=0,1)$ and $E(0^+;v'=0)$ levels with relative intensities in accord with a 300 K Boltzmann weight are also shown in Fig. 11. From the comparison, the $D'(2)$-$A'\ ^3\Pi_2$ bands can be identified. Assuming similar radiative lifetimes, the relative intensities of the $D'(2)$, $\beta(1)$, and $E(0^+)$ transitions suggest that $T_0(D')$-$T_0(\beta)$ is $\sim$10 cm^{-1}. If we adopt the same vibrational numbering for the $D'(2)$-$A'\ ^3\Pi_2$ bands as for the $\beta(1)$-$A^3\Pi_1$ bands (Fig. 11), the blue shift of the $D'(2)$ bands, relative to the $\beta(1)$ bands, suggests that the $A'\ ^3\Pi_2$ state is $\sim$100 cm^{-1} below the $A\ ^3\Pi_1$ state.

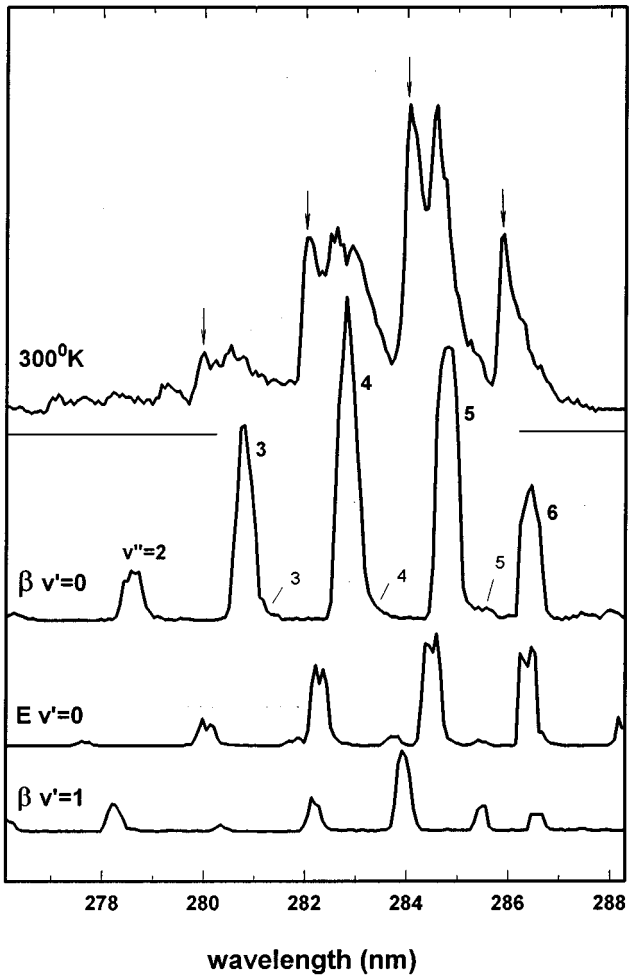

FIG. 11. High pressure emission spectrum from the ion-pair states of ClF for 300 K Boltzmann conditions. The individual emission spectra with a Boltzmann weighing of intensities from $\beta(1)$, $v'=0,1\rightarrow A\ ^3\Pi_1$, v'' and $E(0^+)$, $v'=0\rightarrow B\ ^3\Pi_{0+}$, v'' are shown for reference. The main features that can be assigned as $D'(2)\rightarrow A'\ ^3\Pi_2$ bands are marked by the arrows. The weak band marked as 3, 4, and 5 are the $\beta(1)$, $v'=0\rightarrow B\ ^3\Pi_{0+}$, $v''=3$, 4, and 5 transitions that are observed as a consequence of the heterogenous perturbation between $\beta(1)$ and $E(0^+)$.

V. CONCLUSIONS

Strong homogeneous interactions between the $\Omega=1$ and 0^+ pairs of states lead to irregular vibrational spacings and rotational constants for the first eight vibrational energy levels in each of the $\beta(1)$, $G(1)$, $E(0^+)$, and $f(0^+)$ ion-pair states of ClF. This intriguing situation invites a deperturbation analysis based on a model involving the interaction of many vibrational levels. In order to proceed with such an

analysis, experimental results for less severely perturbed Cl^+F^- states are needed to provide the zeroth order potentials; the f sublevels of the $\beta(1)$ state or the $D'(2)$ state are likely candidates for less unperturbed states. The new information presented here for the $A\ ^3\Pi_1$ and $A'\ ^3\Pi_2$ valence states should facilitate experiments to investigate the remaining ion-pair states.

In addition to the bound-bound emission spectra from the ion-pair states that were analyzed in this work, numerous bound-free transitions also were observed. In the future, we hope to interpret these spectra to obtain more information about the repulsive valence potentials of ClF.[12] Certain vibrational levels in the $E(0^+)$ and $f(0^+)$ states emit to very high levels of ClF ($X\ \Sigma^+$), and the ground state potential could be improved by an analysis of these data. Our original interest, the interaction between the Rydberg and ion-pair states, also remains to be investigated. Clearly, a great deal remains to be learned about the excited electronic states of the interesting ClF molecule.

ACKNOWLEDGMENTS

This work was supported by the National Science Foundation under Grant W. CHE-9505032. We thank Dr. Helene Lefebvre–Brion for reading the manuscript and offering constructive comments. We also thank Jan Vaughan for her expert assistance in the preparation of this manuscript.

[1] (a) T. Ishiwata, J. Si, and K. Obi, J. Chem. Phys. **96**, 5678 (1992); (b) T. Ishiwata, Y. Kasqi, and K. Obi, *ibid*. **98**, 3620 (1993); (c) T. Shinzawa, A. Tokunaga, T. Ishiwata, and I. Tanaka, *ibid*. **83**, 5407 (1985); (d) T. Ishiwata, T. Shinzawa, J. Si, K. Obi, and I. Tanaka, J. Mol. Spectrosc. **166**, 321 (1994).

[2] (a) J. Wormer, T. Moller, J. Stapelfeldt, G. Zimmerer, D. Haaks, S. Kampf, J. Le Calvé, and M. C. Castex, Z. Phys. D **7**, 383 (1988); (b) T. Moller, B. Jordan, P. Gurtler, G. Zimmerer, D. Haaks, J. LeCalvé, and M. C. Castex, Chem. Phys. **76**, 295 (1983).

[3] (a) P. Wang, S. S. Dimov, G. Rosenblood, and R. H. Lipson, J. Phys. Chem. **99**, 3984 (1995); (b) M. S. N. Al-Kahali, R. J. Donovan, K. P. Lawley, T. Ridley, and A. J. Yarwood, *ibid.* **99**, 3978 (1995).

[4] S. D. Peyerimhoff and R. J. Buenker, Chem. Phys. **57**, 279 (1981).

[5] (a) J. C. D. Brand, A. R. Hoy, and A. C. Risbud, J. Mol. Spectroc. **113**, 47 (1985); (b) J. C. D. Brand and A. R. Hoy, Appl. Spectrosc. Rev. **23**, 285 (1987); (c) J. C. D. Brand, A. R. Hoy, and S. M. Jaywant, J. Mol. Spectrosc. **106**, 388 (1984); (d) J. C. D. Brand, U. D. Deshpande, A. R. Hoy, and S. M. Jaywant, *ibid*. **100**, 416 (1983).

[6] (a) R. I. Narayani and J. Tellinghuisen, J. Mol. Spectrosc. **141**, 79 (1990); (b) D. T. Radzykewycz, C: D. Littlejohn, M. B. Carter, J. O. Clevenger, J. H. Purvis, and J. Tellinghuism, *ibid*. **166**, 287 (1994); (c) X. Zhang, M. C. Heaven, and J. Tellinghuisen, *ibid*. **104**, 135 (1994); (d) M. A. Stepp, M. A. Kremer, P. C. Tellinghuisen, and J. Tellinghuisen, *ibid*. **146**, 169 (1991); (e) S. W. Brown, C. J. Dowd, Jr., and J. Tellinghuisen, *ibid*. **132**, 178 (1988).

[7] K. P. Lawley, E. A. Kerr, R. J. Donovan, A. Hopkirk, D. Shaw, and A. J. Yencha, J. Phys. Chem. **94**, 6201 (1990).

[8] R. H. Lipson and A. R. Hoy, J. Chem. Phys. **90**, 6821 (1989).

[9] F. Alberti, K. P. Huber, and E. C. Looi, J. Mol. Spectrosc. **102**, 289 (1983).

[10] K. Darvesh, R. J. Boyd, and S. D. Peyerimhoff, Chem. Phys. **121**, 361 (1988).

[11] (a) K. Lawley, P. Jewsbury, T. Ridley, P. Langride-Smith, and R. Donovan, Mol. Phys. **75**, 811 (1992). This paper gives a good summary of allowed transitions and the molecular orbital description for the spectroscopic states of I_2; (b) K. Balasubramanian, Chem. Phys. **119**, 41 (1988).

[12] V. Alekseev and D. W. Setser (unpublished).

[13] (a) I. S. McDermid, J. Chem. Soc. Faraday Trans. II **77**, 519 (1981); (b) I. S. McDermid and J. B. Laudenslanger, Chem. Phys. Lett. **79**, 370 (1981); (c) W. Stricker and L. Krauss, Z. Naturforsch. A **23**, 1116 (1968); (d) A. C. Wahrhaffig, J. Chem. Phys. **10**, 248 (1942).

[14] (a) H. Lefebvre-Brion and R. W. Field, *Perturbations in the Spectra of Diatomic Molecules* (Academic, New York, 1986); see Table 2.6 on page 85; (b) D. Stahel, M. Leoni, and K. Dressler, J. Chem. Phys. **79**, 2541 (1983); (c) See Eq. 2.3.16 of Ref. 15(a) for a complete definition; (d) See Eq. 3.4.34 of Ref. 15(a).

[15] (a) L. Veseth, J. Phys. B **6**, 1473 (1973); (b) D. Bassieres and A. R. Hoy, Can. J. Phys. **62**, 1941 (1984).

[16] M. Diegelman, K. Hohla, F. Rebentrost, and K. L. Kompa, J. Chem. Phys. **76**, 1233 (1982).

[17] M. Diegelman, D. Proch, and Z. Zensheng, Appl. Phys. B. **40**, 49 (1986).